CHAPTER - 5

Metal-molecule interactions: Cystine on copper cluster

5.1 Introduction

Cystine is a dimer formed via oxidation of the thiol head group of amino acid cysteine. Cystine has a disulfide linkage (–S–S–) which is responsible for the folding and unfolding of proteins and thus provides stability to the secondary and tertiary structure of proteins.[1–5] SERS (surface-enhanced Raman scattering) technique has proven highly effective in examining the structural and stability characteristics of this molecule.[6,7] In fact, SERS technique stands out as an exceptionally sensitive surface method for detecting various adsorbate molecules, pushing the boundaries to achieve single molecule detection levels.[8–10] Conventionally, coinage metals such as Au, Ag, and Cu have been preferred substrates due to their ability to substantially boost the Raman scattering signals of molecules adsorbed onto their surfaces.

The significant amplification primarily originates from two mechanisms; electromagnetic field enhancement (EM) and chemical enhancement (CE).[8,11,12] EM enhancement primarily arises when surface plasmon resonance occurs on a metal surface[13,14] whereas, CE enhancement is ascribed to a resonance-like process involving charge transfer between the substrate and the probe molecule.[15–17] Unlike the electromagnetic (EM) mechanism, the chemical enhancement (CE) mechanism requires the adsorbate to be in close proximity to the SERS substrate. While both mechanisms can play a role in enhancing SERS simultaneously, the degree of SERS enhancement also relies on experimental factors, the composition and structure of the SERS substrate, and the characteristics of the specific analyte.[18–20]

The stability of disulfide in the chemisorbed cystine on silver and gold nanoparticles was studied experimentally, in which it was found that the disulfide bond remained intact on large-sized gold nanoparticles while it was cleaved on smaller gold nanoparticles.[21] At a lower concentration of cystine, the disulfide bond got cleaved, while at higher concentration, this cleavage was prevented by a monodentate binding of cystine on to the silver metal surface (nanoparticles). It was also shown that the adsorption through

disulfide caused cleavage of this linkage after which cystine got adsorbed either through its thiol/ carboxylic or thiol/amino or amino/carboxylic groups on the metal surface.

SERS measurements of cystine adsorbed on copper metal revealed that on bulk copper the disulfide bond remained intact, whereas it got cleaved when adsorbed on copper nanoparticles.[22] The mechanism of breaking of the disulfide bond on copper nanoparticles and the role of other functional groups of cystine toward its interaction with copper metal are yet to be understood. According to the literature reported, DFT (density functional theory) methods have been found to be very efficient in predicting the interaction between adsorbed molecule/moiety and metal surfaces.[23–26]

Recently, T.D. Hieu et al. studied SERS of thiram pesticide on copper cluster by DFT method and found that their predictions supported the experimental results exceedingly well.[27] Small-sized copper clusters were found as efficient model clusters to represent the metal surface for the study of adsorption as shown by Ahmed et al.[28] Literature revealed that the model surface clusters provide an optimal extrapolation to the properties of the metal surface.[29]

Therefore, in this chapter DFT method was used to get better insight about the binding modes between cystine and metal cluster comprising 9 copper atoms (Cu9). Computational characterization of the adsorption of cystine on the copper cluster has not been reported earlier, to the best of our knowledge. Computational results reported herein substantiate the earlier reported experimental finding significantly well.[22] This study also suggested that, unlike Ag and Au metals, Cu metal not only shows affinity toward sulfur but also toward oxygen also, rendering Cu a very good SERS substrate despite being air sensitive.

5.2 Computational Details

Using the molecule-model approach, a 9-atom copper cluster (Cu9) was constructed by the Avogadro software.[30] The Gaussian 16 program package was employed for the DFT calculations. Ground-state optimization was carried out for cysteine, Cu9 cluster. The

optimized geometries were used to create the cystine-Cu9 (Cys-Cu9) system which was further subjected to geometry optimization. Normal mode and relative Raman activity were calculated for the optimized geometries. The MK (Merz Kollman), ESP (electrostatic potential) charges of each atom, and FMO (frontier molecular orbital) calculations were carried out to determine the stability of the Cys-Cu9 system. NBO (natural bond orbital) and AIM (atoms in molecule) calculations were performed to find out the extent of interaction between cystine and Cu9 cluster. For the investigation of DOS (density of states), Multiwfn was utilized. Becke's three-parameter functional and Lee–Yang–Parr hybrid functional (B3LYP) was used for all the above calculations and Cu atoms were treated by relativistic effective core potentials (RECP) with (LANL2DZ),[31] and for C, H, N, S, and O atoms 6–311+ +G(d,p) basis set was used. The tight convergence criterion of Gaussian 16 was used in structural optimization. The geometry of the Cys-Cu9 system was fully optimized without any constraint on the geometry. It was also reported that usually cystine occurred in its zwitterionic form in solution.[21,22] Hence, in this work, the zwitterionic form of cystine where the carboxyl group was considered in its de-protonated state and protonated amine group was taken. The implicit solvation model[32] based on density in Gaussian 16 package was employed for the calculations of both the energy and vibrational properties.

5.3 Results and discussion

5.3.1 Geometry optimization

Different orientations of cystine toward copper cluster were taken for geometry optimization in order to probe the binding modes between cystine and Cu cluster and thereby resulting in the most stable CysCu9 system. These different orientations were designated as Cys-Cu(A), Cys-Cu(B), Cys-Cu(C), and Cys-Cu(D), where Cys-Cu represents the Cys-Cu9 system while (A), (B), (C), and (D) represents different orientations of cystine toward copper cluster. All the optimized structures were found to be global minimum having no imaginary frequency. The optimized structures are shown

in Fig. 5.1. The interaction energy was calculated for all four Cys-Cu9 systems at B3LYP/LANL2DZ/6–311+ +G(d,p) level of theory using the following equation (1):

$$\text{Interaction energy} = E_{Cu9-cystine} - E_{Cu9} - E_{cystine} \quad (1)$$

where $E_{Cu9\text{-}cystine}$ refers to the optimized energy of the Cu9-cystine system, E_{Cu9} refers to the optimized energy of the Cu9 cluster, and $E_{cystine}$ refers to the optimized energy of the cystine molecule. It was observed that the system Cys-Cu(A) had the highest interaction energy compared to other systems and are mentioned in the caption of Fig. 5.1. Interaction energy was also calculated at the other level of theory (shown in figure 5.2), and among all, the B3LYP/LANL2DZ/6–311+ +G(d,p) level of theory was found to be the optimal one. Therefore, throughout this study B3LYP/LANL2DZ/6–311+ + G(d,p) level of theory was utilized. As the highest interaction energy was observed in Cys-Cu(A) system, it was used for further analyzing the interaction between cysteine and Cu9 in detail.

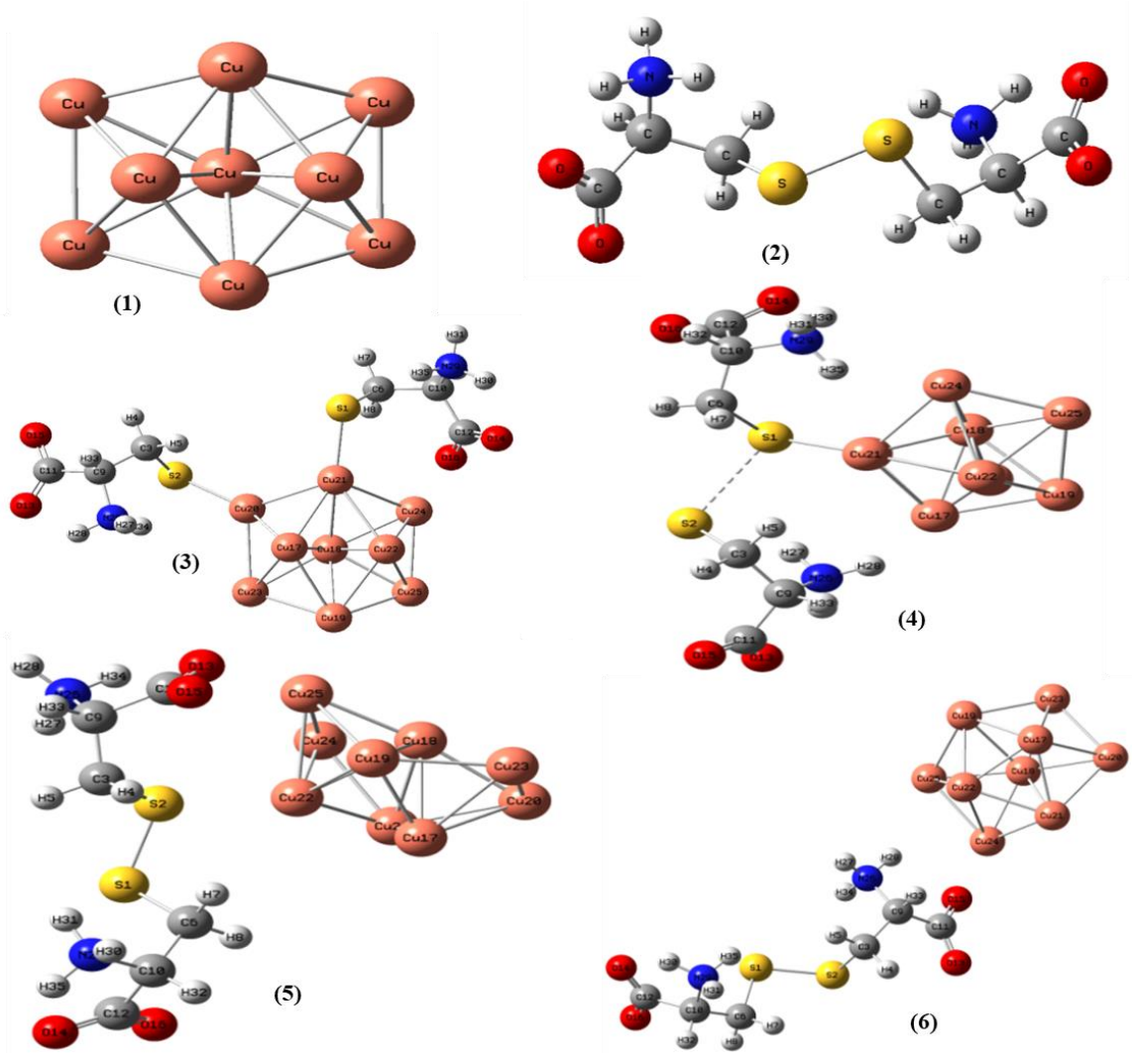

Figure 5.1: Optimized structures at B3LYP/LANL2DZ/6–311+ +G(d,p) level of theory: 1 Cu9 cluster, 2 cystine, 3 Cys-Cu(A) with interaction energy (IE)= −88.34 kcal/mol, 4 Cys-Cu(B) with IE= −40.28 kcal mol, 5 Cys-Cu(C) with IE= −23.84 kcal/mol, and 6 Cys-Cu(D) with IE= −19.51 kcal/mol [atoms in Cys-Cu9 are numbered]

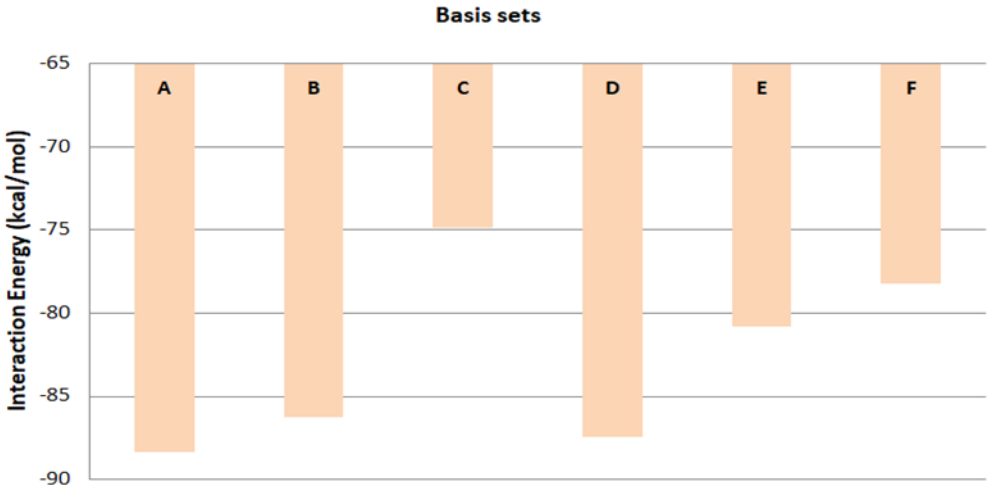

Figure 5.2: Interaction energy in kcal/mol at B3LYP functional but different basis sets

where, A = LANL2DZ/6-311++G(d,p), B = LANL2DZ/6-311++G(2d,2p), C = LANL2DZ/cc-pVDZ, D = LANL2DZ/cc-pVTZ, E = Def2-TZVPP and F = SDD/6-311++G(d,p)

5.3.2 Vibrational analysis

By comparing normal Raman spectra and SERS spectra of cysteine, the effect of the copper cluster on cystine molecule was apparent through the peak shift. Raman frequencies were calculated for both cystine and Cys-Cu(A) system at B3LYP/LANL2DZ/6–311+ +G(d,p) level of theory. Calculated normal modes of vibrations were assigned by visualizing modes on the Gauss view 6.0.16 platform. The comparison of experimental and calculated Raman vibrational frequencies along with the simulated SERS of cysteine on Cu9 cluster is shown in Table 5.1. Some specific peaks are marked in the calculated Raman and SERS spectrum of cysteine, shown in Fig. 5.3.

Table 5.1: Calculated and Experimental Raman active normal modes of vibrations of cystine at B3LYP/LANL2DZ/6-311++G(d,p) level of theory

Calculated SERS modes of Cystine on Cu9 cluster (cm^{-1})	**Calculated Raman modes of Cystine (solvent) (cm^{-1})**	**Experimental Raman modes of Cystine Solid (cm^{-1})[22]**	**#Tentative Assignment**
282	-	-	ν(Cu-S)
307	-	-	ν(Cu-S)
327	-	-	ν(Cu-O)
-	518	497	ν_s(S-S)
671	666	614	ν(C-S)
1021	1035	-	ν(C-N)
1356	1354	1338	ν(C-C)
1397	1378	1407	β(C-H)+ ν(COO^-)
1577	1608	-	δ(NH_3)
1639	1673	-	ν_{as}(COO^-)+δ(NH_3)
3061	3095	2913	ν_s(C-H)
3135	3155	2966	ν_{as}(C-H)

#Note: (ν) = stretching, (ν_s) = symmetric stretching, (ν_{as}) = asymmetric stretching, (δ) = bending and (β) = out of plane bending

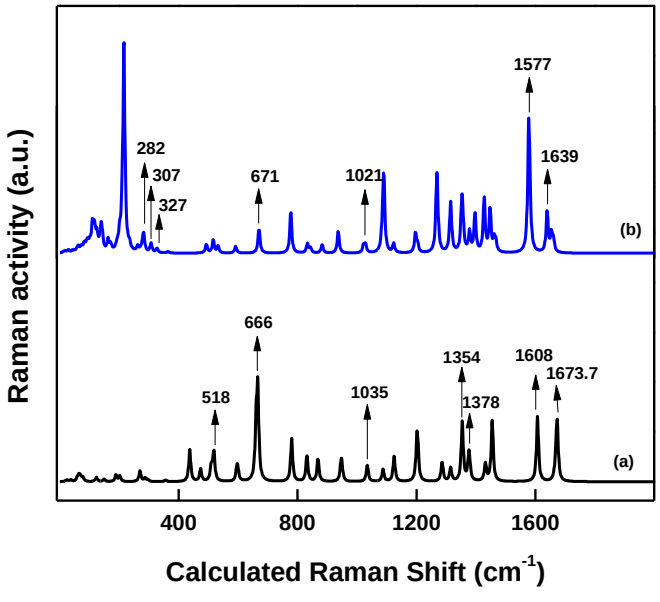

Figure 5.3: Calculated Raman Spectrum; (a) cystine and (b) Cys-Cu(A) system

It is inferred from the Raman spectrum (Fig. 5.3) that the disulfide linkage of cystine got cleaved after interacting with the Cu9 cluster. The band which appears at 518 cm^{-1} due to S–S stretching vibrational mode of cystine got completely disappeared after interacting with the Cu9 cluster. This indicates a strong interaction with Cu9 via its disulfide linkage. This observation was also reported in an earlier experimental study,[22] wherein it was reported that the disulfide bond of cystine got cleaved completely when it was adsorbed on copper nanoparticles through SERS studies. Blue shift in C–S stretching vibrational mode can be attributed (Fig. 5.3, Table 5.1) to the strengthening of the S–C bond. This observation, too, was found in good agreement with the earlier reported experimental study.[22] In the calculated SERS spectrum reported herein, the red shift observed in the asymmetric stretching vibrational mode of $CO2^{-}$ from 1673.7 [cystine] to 1639 cm^{-1} [Cys-Cu(A) system] indicates a strong interaction of carboxylate with the Cu9 cluster. Besides these, peaks corresponding to the stretching modes of Cu–S were predicted at 282 cm^{-1}, 307 cm^{-1}, and the Cu–O stretching was predicted at 327 cm^{-1}. Expectedly, owing to the plasmonic resonance, most Raman peaks of cystine got intensified suggesting a strong interaction between cystine and copper cluster.

These observations further support the experimental findings that the disulfide linkage got cleaved on copper cluster. The interaction between cystine and copper cluster is also stabilized by the carboxylic moiety. Raman frequency calculation provides the reason behind the change in the bond length observed in the optimized structure of cystine prior to and after being adsorbed on the copper cluster (Table 5.2). The disappearance of a symmetric stretching mode of the disulfide confirms the cleavage of a disulfide bond. Similarly, an increase in the bond length of C=O and N–H bonds got confirmed by the red shift in δ_{NH3+} and $\nu_{as}CO2-$ vibrational modes. These observations were also supported by NBO results where electron pair donation from sulfur to Cu caused its cleavage. Similarly, the electron pair donation from oxygen to Cu weakened the C=O bond, resulting in the red shift of the $\nu_{as}CO2^{-}$ vibrational mode. And the decrease in bond distance between S and Cu and O and Cu also suggests its interaction toward Cu cluster which is confirmed by the appearance of Cu–S and Cu–O bands in Raman frequency

calculation. Consequently, these observations, too, emphasized that the adsorption of cystine on copper cluster occurs via cleavage of its disulfide linkage.

Table 5.2: Calculated bond length (Å) of Cys-Cu(A) system at B3LYP/LANL2DZ/6-311++G(d,p) level of theory

Bonds [##]	Bond length (Å)	
	Pre-adsorption	**Post-adsorption**
S1-S2	2.08	5.28
S1-C3	1.85	1.85
C12-O16	1.21	1.27
S1-Cu21	2.58	2.29
S2-Cu20	3.34	2.26
O16-Cu24	5.56	1.99

[##] Atom numbering according to the optimized geometry shown in figure 5.1(3)

From table 5.2 it is inferred that in Cys-Cu(A) system, the difference in bond lengths was observed after adsorption of cystine on copper cluster. The bond distance between S-S got increased from 2.089 to 5.277 Å suggesting the cleavage of the disulfide linkage (-S-S-). Also the bond distance between Cu-S and Cu-O got reduced after adsorption. These observations are well supported by Raman frequency calculations.

5.3.3 DOS (density of states) analysis

From the total density of states (TDOS) plots shown in Fig. 5.4, it is inferred that the energy band gap of the Cu9 cluster got reduced from 2.20 to 1.24 eV, after interacting with cystine. This reduced band gap, besides indicating a stronger interaction between the Cu9 cluster and cysteine, confirms the transfer of electron density from cystine to the Cu9 cluster along with a back donation from the cluster to cystine. From the analysis of the projected density of states (PDOS), it was observed that in the highest occupied molecular orbital (HOMO) of the Cu9-cystine, the contribution of cystine is about 60% while Cu9 contribution is about 40%. Similarly, the lowest unoccupied molecular orbital (LUMO) of Cu9-cystine consists of 90% contribution from Cu9 while 10% contribution

from the cystine molecule. It means 50% electron density is transferred from cystine to Cu9 cluster during the transition from HOMO to LUMO of the Cys-Cu(A) system.

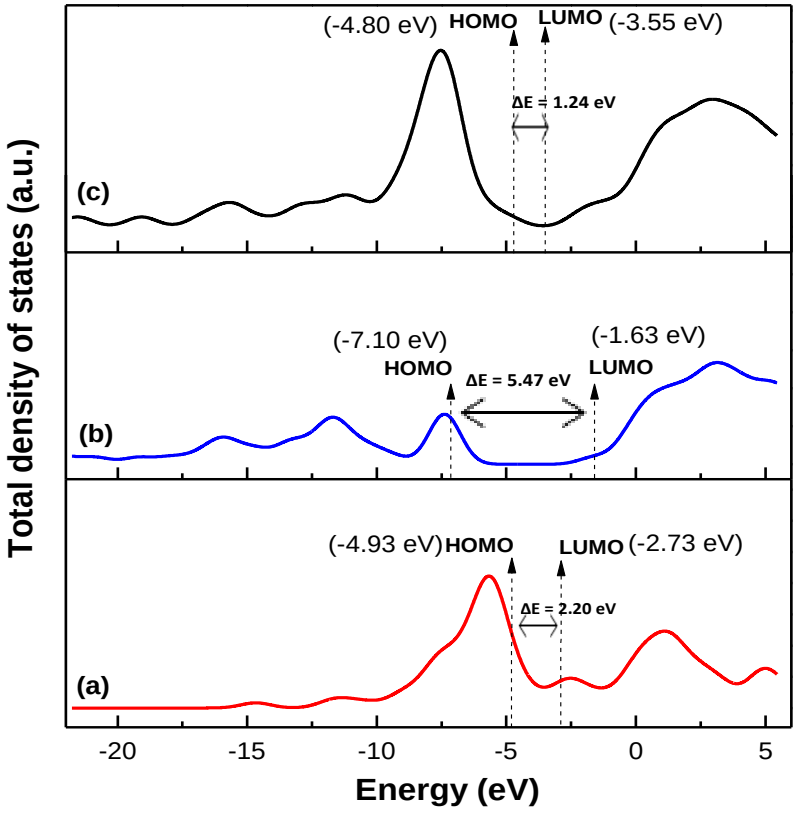

Figure 5.4: Total density of plot of (a) Cu9 cluster (b) Cystine and (c) Cys-Cu(A) system showing energy of HOMO, LUMO and band gap (ΔE)

5.3.4 NBO analysis

NBO analysis has been found to be very effective and accurate for determining the charge transfer and its strength. It provides the stabilization energy E(2) which is estimated by second-order perturbation theory. The detail is given in the introduction section 1.6.3.

This stabilization energy E(2) is associated with the delocalization of electron pair from donor orbital to acceptor orbital. As E(2) increases the interaction between the donor and acceptor orbitals will be greater and, consequently, the strength of the interaction will also be higher. Therefore, to get more insight about which orbitals are involved in these charge transfer and their strength, NBO calculation was carried out for the Cys-Cu(A)

system at B3LYP/ LANL2DZ/6–311+ +G (d, p) level of theory. Some significant donor–acceptor NBO interactions in CysCu(A) system are shown in Table 5.3. From NBO analysis, it was observed that the sulfur atoms are donating its electron pair to the antibonding (dσ) orbital of Cu with high E(2) stabilization energy. Similarly, the oxygen atom is also donating its electron pair to the antibonding (dσ) orbital of Cu. Due to this electron transfer, the negative charge density on sulfur and oxygen atoms decreases which is confirmed by the MK[ESP] charge calculation. It is hereby inferred that the disulfide linkage and carboxylate groups of cystine molecule majorly interact with the cluster and thereby adding stability to the system.

Table 5.3: Some significant donor-acceptor NBO interactions in Cys-Cu(A) system with calculated second-order stabilization energies E(2) (kcal/mol)

Donor NBO→ Acceptor NBO$	**E(2) kcal/mol**
LP S1 → LP* Cu21	4.61
LP O16 → LP* Cu24	9.76
LP S2 → LP* Cu20	6.40
LP* Cu20 → BD* C3 – H4	1.60
LP O13 → BD* N26 – H28	4.68
LP* Cu21 → BD* S2 – Cu20	9.33
BD C10 – C12 → LP* Cu24	2.92

$: BD-Bonding orbital, BD*-antibonding orbital, LP-lone pair of electrons, LP*-dπ-orbital of Cu atom. Atom numbering according to the optimized geometry shown in figure 5.1(3).

5.3.5 AIM analysis

While carrying out Bader's topological AIM analysis, the nature of bonding interaction was analyzed by means of properties of electron density and its derivatives. The theory of AIM analysis is given in introduction section 1.6.4. In the AIM analysis of Cys-Cu(A) (table 5.4 and figure 5.5), it was observed that the interaction between S and Cu is of medium strength having partially covalent character, while between O and Cu, the interaction is weak and non-covalent kind. Besides weak non-covalent H-bond interactions were also observed, as shown in Table 5.4. The equation formulated by Emamian et al.[33] was used to compute these interaction energies. Thus, it can be

concluded that bond between S and Cu can be considered partially covalent and partially electrostatic, which further reinforced the cleavage of disulfide linkage in cystine. At BCP (3,−1) the calculated parameters of AIM analysis are summarized in Table 5.4 and basin surfaces of corresponding BCP are shown in figure 5.5.

Table 5.4: Topological parameters for bonds of interacting atoms in Cys-Cu(A) system: electron density (ρ_{BCP}), kinetic electron energy density (G_{BCP}), potential electron energy density (V_{BCP}), total electron energy density (H_{BCP}), Laplacian of electron density (∇^2_{BCP}), estimated interaction energy (E_{int}) at bond critical point (BCP)

Critical Point number	**ρBCP (a.u.)**	**G_{BCP} (a.u.)**	**V_{BCP} (a.u.)**	**H_{BCP} (a.u.)**	**$\nabla^2\rho BCP$ (a.u.)**	**E_{int} (kcal/mol)**
14(O→HN)	0.03703	0.02880	-0.02842	0.00032	0.11649	-7.51
24(S→HN)	0.02038	0.01204	-0.01144	0.00060	0.05058	-3.80
33(S→Cu)	0.07089	0.06952	-0.07773	-0.00820	0.24526	-15.1
38(O→Cu)	0.07031	0.12268	-0.11828	0.00439	0.50833	-14.94
39(S→Cu)	0.06542	0.06759	-0.07348	-0.00589	0.24680	-13.85
46(O→HN)	0.02848	0.02382	-0.02104	0.00277	0.10639	-5.61
48(S→HN)	0.02254	0.01290	-0.01281	0.00009	0.05200	-4.3

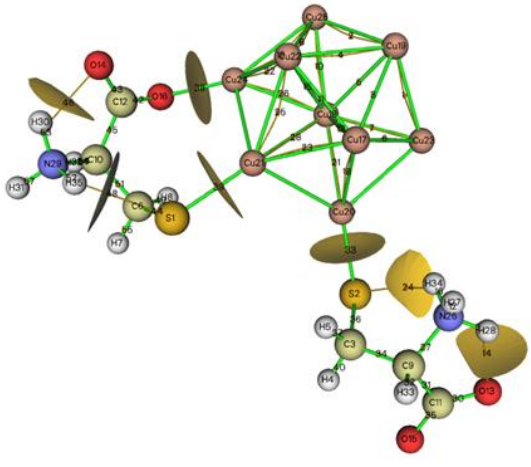

Figure 5.5: Topological basin surfaces with Bond critical points (3,-1) of Cys-Cu(A) system at B3LYP/LANL2DZ/6-311++G(d,p) level

5.3.6 FMO analysis

FMO calculations were reported to provide deeper insight on the chemical reactivity and stability of a system. Ground state properties of Cys-Cu(A) system were utilized for calculating the FMO at B3LYP/ LANL2DZ/6–311+ +G(d,p) level of theory. With the help of FMO results, the global reactivity descriptors like μ (chemical potential), η (chemical hardness), χ (electronegativity), and ω (electrophilicity index) were calculated using equations as given in the introduction section 1.6.6.

In the present study, the reduced HOMO–LUMO gap in Cys-Cu(A) indicates the increased reactivity of cystine after adsorption on copper cluster. The high dipole moment of 25.81D indicates a substantial charge rearrangement in the system Cys-Cu(A). The low value of hardness suggests the increased reactivity of cystine on copper cluster. Similarly, the values of μ, χ, and ω, too, support the above prediction. The frontier molecular orbitals and all the calculated energy parameters of FMOs for cluster, cysteine, and CysCu(A) system are shown in figure 5.6 and table 5.5.

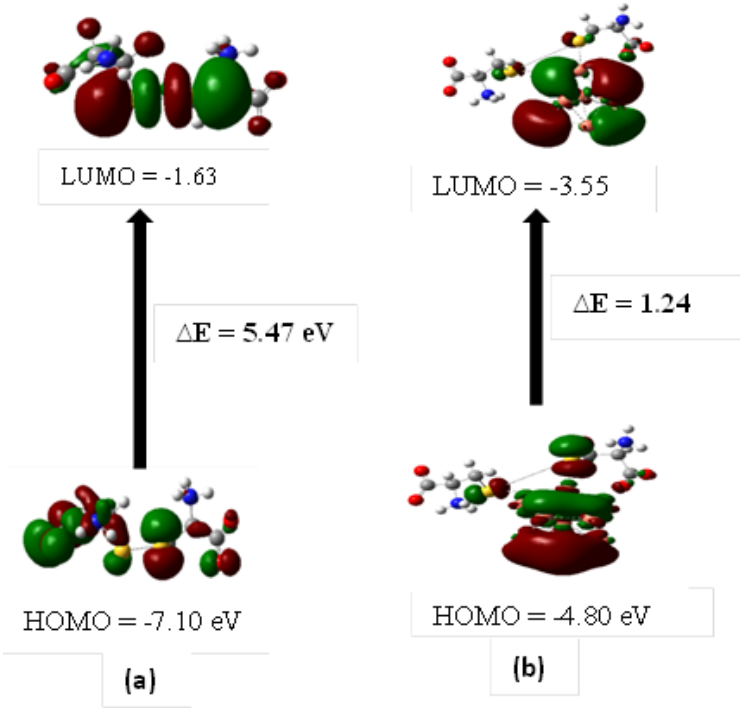

Figure 5.6: HOMO-LUMO (ΔE) gap of (a) cystine (b) Cys-Cu(A) system

Table 5.5: Computed energy [eV] parameters at B3LYP/cc-PVTZ level of theory

Energy Parameters	**Cu9**	**Cystine**	**Cys-Cu(A) system**
E_{HOMO} (IP) [eV]	-4.93	-7.10	-4.80
E_{LUMO} (EA) [eV]	-2.73	-1.63	-3.55
HOMO-LUMO gap (Eg) [eV]	2.20	5.47	1.24
Dipole moment [D]	0.08	15.75	25.81
Hardness(η) [eV]	-3.83	-4.36	-4.17
Chemical potential(μ) [eV]	-1.10	-2.73	-0.63
Electronegativity(χ) [eV]	-3.83	-4.36	-4.17
Electrophilicity index(ω) [eV]	-0.16	-0.85	-0.05

5.3.7 Charge analysis

Interaction of copper cluster with cystine molecule affects the charge distribution of these independent moieties. These charge values can be calculated by Merz Kollman (MK) electrostatic potential (ESP) charge calculations. According to the literature, charges calculated using the MK scheme are better compared to the Mulliken scheme as the former is almost invariant to the level of theory and basis sets,[34] in contrast to the latter. Therefore, MK[ESP] charge calculation was performed for Cu9, cystine, and Cys-Cu(A) system at B3LYP/LANL2DZ/6–311+ +G(d,p) level of theory. The charge values, before and after adsorption, on each atom of Cu cluster and cystine are shown in table 5.6 and figure 5.7. It was observed that the negative charge on S1 decreased from −0.124 to 0.087 a.u. upon interaction with the Cu cluster. Similarly, the negative charges on all oxygen and nitrogen atoms decreased which indicate that these atoms interact with the Cu9 cluster.

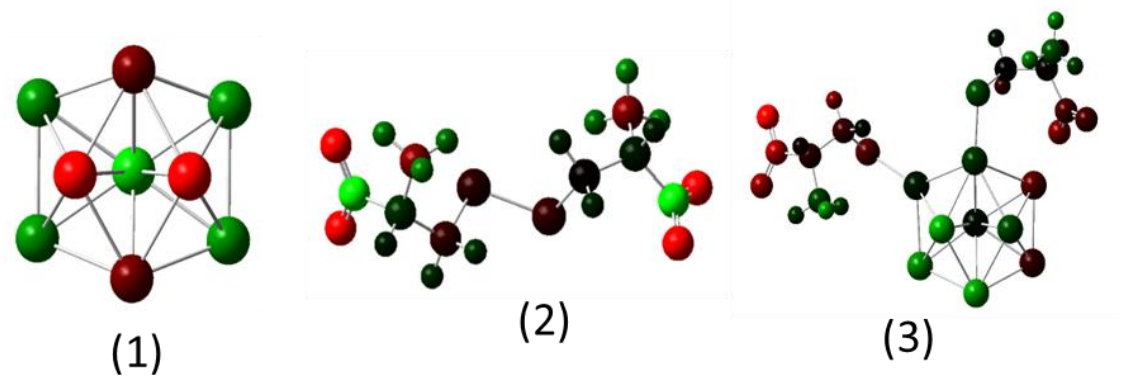

Figure 5.7: ESP charge density shown by colour (1) Cu9, (2) cystine and (3) Cys-Cu(A) system; where, ● represents extreme negative charge (a.u.) and ● represents extreme positive charge (a.u.) and the charges in between them are represented by other colours shown in this figure

Table 5.6: Results of MK[ESP] charge calculation at B3LYp/LANL2DZ/6-311++G(d,p) level of theory

Atoms	**Charges on atoms (a.u.)**		**##ΔQ(a.u.)**
	Post adsorption	**Pre adsorption**	
S1	0.087	-0.124	-0.211
S2	-0.101	-0.145	-0.044
O13	-0.170	-0.775	-0.604
O14	-0.080	-0.780	-0.699
O15	-0.344	-0.773	-0.428
O16	-0.149	-0.779	-0.629
Cu17	0.201	-0.003	-0.205
Cu18	0.015	0.002	-0.013
Cu19	0.190	-0.001	-0.191
Cu20	0.028	0.001	-0.027
Cu21	0.061	-0.001	-0.063
Cu22	0.084	-0.003	-0.087
Cu23	0.163	0.001	-0.162
Cu24	-0.103	0.001	0.104
Cu25	-0.066	0.001	0.068
N26	0.077	-0.366	-0.444
N29	0.097	-0.363	-0.460

ΔQ = represents differences in charges on each atom before and after adsorption, numbers after atoms represents the label of that atom in optimized geometry of Cys-Cu(A) system

From the table 5.6 and figure 5.7, it is inferred that the negative charge on sulfur moieties decreased after adsorption of cystine on copper cluster. Similarly, the negative charges on all oxygen and nitrogen atoms decreased which indicate that these atoms interact with the Cu9 cluster.

The distribution of charge density on Cys-Cu(A) system is depicted in Fig. 5.8, where it is evident that the carboxylate moiety directed toward cluster has electron density, while the one which is away from cluster has comparatively more. Also, there is less electron density on sulfur moieties indicating the chemisorption of cystine via sulfur moieties.

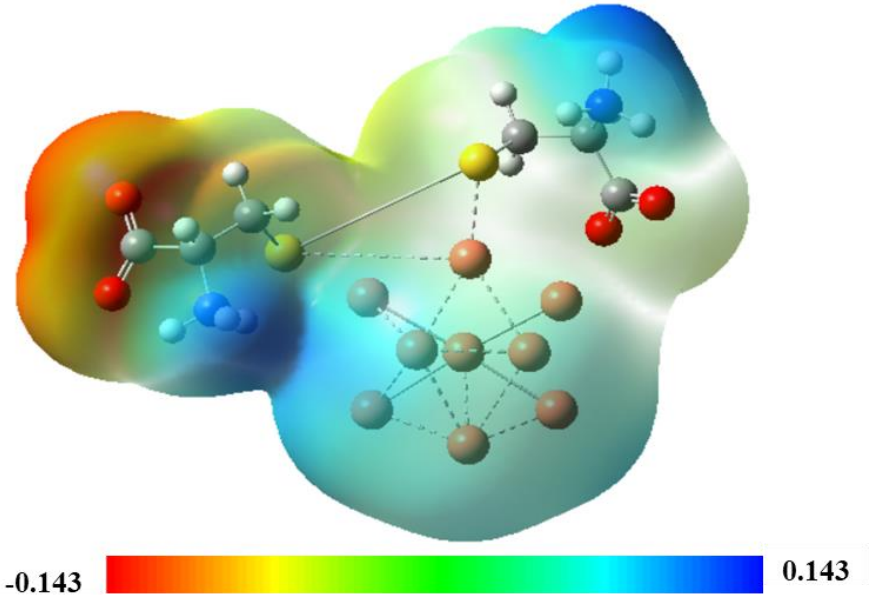

Figure 5.8: ESP Map on Cys-Cu(A) system. The colour scale indicates red as minimum electrostatic potential meaning excess of electrons or loosely bound electrons and blue as the maximum of electrostatic potential.

5.4 Conclusion

Structural, electronic, and spectral properties of cystine and its complex with Cu9 cluster were investigated using DFT method. The interaction energy between cystine and Cu cluster was observed to be −88.34 kcal/mol in Cys-Cu(A) system where disulfide linkage got cleaved completely. In calculated SERS of cystine on Cu9 cluster, the cleavage of disulfide linkage was confirmed by the disappearance of the S–S stretching vibrational mode and the blue shift in C–S stretching mode suggest the strong interaction between cystine and copper cluster. Involvement of the carboxyl moiety in interacting with the Cu9 cluster was also significant. These observations are in good agreement with earlier reported experimental findings. NBO and PDOS analysis revealed that electron density got transferred from cystine molecule to copper cluster along with a back donation from cluster to molecule, thereby contributing to the overall stability of the system. AIM analysis revealed the partial covalent and partial electrostatic nature of the Cu–S bond. Results of FMO and MK[ESP] charge calculations supported the above mentioned results exceedingly well. Thus, from the present computational study, it is reinforced that cystine got chemisorbed on copper cluster via the cleavage of its disulfide linkage.

5.5 References

(1) Sevier, C. S.; Kaiser, C. A. Formation and Transfer of Disulphide Bonds in Living Cells. *Nat. Rev. Mol. Cell Biol.* **2002**, *3* (11), 836–847.

(2) Betz, S. F. Disulfide Bonds and the Stability of Globular Proteins. *Protein Sci.* **1993**, *2* (10), 1551–1558.

(3) Matsumura, M.; Signor, G.; Matthews, B. W. Substantial Increase of Protein Stability by Multiple Disulphide Bonds. *Nature* **1989**, *342* (6247), 291–293.

(4) Creighton, T. E. [5] Disulfide Bonds as Probes of Protein Folding Pathways. In *Methods in enzymology*; Elsevier, 1986; Vol. 131, pp 83–106.

(5) Wedemeyer, W. J.; Welker, E.; Narayan, M.; Scheraga, H. A. Disulfide Bonds and Protein Folding. *Biochemistry* **2000**, *39* (15), 4207–4216.

(6) Cotton, T. M.; Kim, J.-H.; Chumanov, G. D. Application of Surface-Enhanced Raman Spectroscopy to Biological Systems. *J. Raman Spectrosc.* **1991**, *22* (12), 729–742.

(7) Garcia-Ramos, J.; Sanchez-Cortes, S. Metal Colloids Employed in the SERS of Biomolecules: Activation When Exciting in the Visible and near-Infrared Regions. *J. Mol. Struct.* **1997**, *405* (1), 13–28.

(8) Moskovits, M. Surface-Enhanced Spectroscopy. *Rev. Mod. Phys.* **1985**, *57* (3), 783.

(9) Kneipp, K.; Wang, Y.; Kneipp, H.; Perelman, L. T.; Itzkan, I.; Dasari, R. R.; Feld, M. S. Single Molecule Detection Using Surface-Enhanced Raman Scattering (SERS). *Phys. Rev. Lett.* **1997**, *78* (9), 1667.

(10) Nie, S.; Emory, S. R. Probing Single Molecules and Single Nanoparticles by Surface-Enhanced Raman Scattering. *science* **1997**, *275* (5303), 1102–1106.

(11) Metiu, H. Surface Enhanced Spectroscopy. *Prog. Surf. Sci.* **1984**, *17* (3–4), 153–320.

(12) Lombardi, J. R.; Birke, R. L. A Unified Approach to Surface-Enhanced Raman Spectroscopy. *J. Phys. Chem. C* **2008**, *112* (14), 5605–5617.

(13) Zeman, E. J.; Schatz, G. C. An Accurate Electromagnetic Theory Study of Surface Enhancement Factors for Silver, Gold, Copper, Lithium, Sodium, Aluminum, Gallium, Indium, Zinc, and Cadmium. *J. Phys. Chem.* **1987**, *91* (3), 634–643.

(14) Aroca, R. *Surface-Enhanced Vibrational Spectroscopy*; John Wiley & Sons, 2006.

(15) Yang, L.; Zhang, Y.; Ruan, W.; Zhao, B.; Xu, W.; Lombardi, J. R. Improved Surface-Enhanced Raman Scattering Properties of TiO2 Nanoparticles by Zn Dopant. *J. Raman Spectrosc.* **2010**, *41* (7), 721–726.

(16) Ji, W.; Xue, X.; Ruan, W.; Wang, C.; Ji, N.; Chen, L.; Li, Z.; Song, W.; Zhao, B.; Lombardi, J. R. Scanned Chemical Enhancement of Surface-Enhanced Raman Scattering Using a Charge-Transfer Complex. *Chem. Commun.* **2011**, *47* (8), 2426–2428.

(17) Musumeci, A.; Gosztola, D.; Schiller, T.; Dimitrijevic, N. M.; Mujica, V.; Martin, D.; Rajh, T. SERS of Semiconducting Nanoparticles (TiO2 Hybrid Composites). *J. Am. Chem. Soc.* **2009**, *131* (17), 6040–6041.

(18) Arenas, J.; López Tocón, I.; Woolley, M.; Otero, J.; Marcos, J. Charge Transfer in SERS: Spectra of 3, 5-Dimethylpyridine at a Silver Electrode. *J. Raman Spectrosc.* **1998**, *29* (8), 673–679.

(19) Bolboaca, M.; Iliescu, T.; Kiefer, W. Infrared Absorption, Raman, and SERS Investigations in Conjunction with Theoretical Simulations on a Phenothiazine Derivative. *Chem. Phys.* **2004**, *298* (1–3), 87–95.

(20) Baia, M.; Baia, L.; Kiefer, W.; Popp, J. Surface-Enhanced Raman Scattering and Density Functional Theoretical Study of Anthranil Adsorbed on Colloidal Silver Particles. *J. Phys. Chem. B* **2004**, *108* (45), 17491–17496.

(21) Lopez-Tobar, E.; Hernández, B.; Ghomi, M.; Sanchez-Cortes, S. Stability of the Disulfide Bond in Cystine Adsorbed on Silver and Gold Nanoparticles as Evidenced by SERS Data. *J. Phys. Chem. C* **2013**, *117* (3), 1531–1537.

(22) Arathi, P.; Seemesh, B.; Ramanathan, V.; others. Disulphide Linkage: To Get Cleaved or Not? Bulk and Nano Copper Based SERS of Cystine. *Spectrochim. Acta. A. Mol. Biomol. Spectrosc.* **2018**, *196*, 229–232.

(23) Foresman, J. Frisch E.(1993). Exploring Chemistry with Electronic Structure Methods, Gaussian. *Inc Pittsburgh*.

(24) Wu, D.; Hayashi, M.; Shiu, Y.; Liang, K.; Chang, C.; Yeh, Y.; Lin, S. A Quantum Chemical Study of Bonding Interaction, Vibrational Frequencies, Force Constants, and Vibrational Coupling of Pyridine- M n (M= Cu, Ag, Au; N= 2- 4). *J. Phys. Chem. A* **2003**, *107* (45), 9658–9667.

(25) Muniz-Miranda, M.; Muniz-Miranda, F.; Caporali, S. SERS and DFT Study of Copper Surfaces Coated with Corrosion Inhibitor. *Beilstein J. Nanotechnol.* **2014**, *5* (1), 2489–2497.

(26) Ferral, A.; Paredes-Olivera, P.; Macagno, V.; Patrito, E. Chemisorption and Physisorption of Alkanethiols on Cu (111). A Quantum Mechanical Investigation. *Surf. Sci.* **2003**, *525* (1–3), 85–99.

(27) Hieu, T. D.; Chinh, N. T.; Nhung, N. T. A.; Quang, D. T.; Quang, D. D. SERS Chemical Enhancement by Copper-Nanostructures: Theoretical Study of Thiram Pesticide Adsorbed on Cu20 Cluster. *Vietnam J. Chem.* **2021**, *59* (2), 159–166.

(28) Ahmed, A. A. Structural and Electronic Properties of the Adsorption of Nitric Oxide Molecule on Copper Clusters CuN (N= 1–7): A DFT Study. *Chem. Phys. Lett.* **2020**, *753*, 137543.

(29) Crispin, X.; Bureau, C.; Geskin, V.; Lazzaroni, R.; Brédas, J.-L. Local Density Functional Study of Copper Clusters: A Comparison between Real Clusters, Model Surface Clusters, and the Actual Metal Surface. *Eur. J. Inorg. Chem.* **1999**, *1999* (2), 349–360.

(30) Hanwell, M. D.; Curtis, D. E.; Lonie, D. C.; Vandermeersch, T.; Zurek, E.; Hutchison, G. R. Avogadro: An Advanced Semantic Chemical Editor, Visualization, and Analysis Platform. *J. Cheminformatics* **2012**, *4* (1), 1–17.

(31) Hay, P. J.; Wadt, W. R. Ab Initio Effective Core Potentials for Molecular Calculations. Potentials for the Transition Metal Atoms Sc to Hg. *J. Chem. Phys.* **1985**, *82* (1), 270–283.

(32) Marenich, A. V.; Cramer, C. J.; Truhlar, D. G. Universal Solvation Model Based on Solute Electron Density and on a Continuum Model of the Solvent Defined by the Bulk Dielectric Constant and Atomic Surface Tensions. *J. Phys. Chem. B* **2009**, *113* (18), 6378–6396.

(33) Emamian, S.; Lu, T.; Kruse, H.; Emamian, H. Exploring Nature and Predicting Strength of Hydrogen Bonds: A Correlation Analysis between Atoms-in-Molecules Descriptors, Binding Energies, and Energy Components of Symmetry-Adapted Perturbation Theory. *J. Comput. Chem.* **2019**, *40* (32), 2868–2881.

(34) Martin, F.; Zipse, H. Charge Distribution in the Water Molecule—A Comparison of Methods. *J. Comput. Chem.* **2005**, *26* (1), 97–105.